Near Surface Geophysics, 2009, 613-627

Spatial mapping of submerged cave systems by means of airborne electromagnetics: an emerging technology to support protection of endangered karst aquifers

Robert Supper[1*], Klaus Motschka[1], Andreas Ahl[1], Peter Bauer-Gottwein[2], Bibi Gondwe[2], Gonzalo Merediz Alonso[3], Alexander Römer[1], David Ottowitz[1] and Wolfgang Kinzelbach[4]

[1] *Geological Survey of Austria, Neulinggasse 38, 1030 Vienna, Austria*
[2] *Department of Environmental Engineering, Technical University of Denmark, Miljovej, Building 113, 2800 Kgs Lyngby, Denmark*
[3] *Amigos de Sian Ka'an, Fuego # 2 Manzana 10 SM 4, Cancún, Quintana Roo, 77500, Mexico*
[4] *Institute of Environmental Engineering, ETH-Zürich, HIL G 37.3, 8093 Zurich, Switzerland*

Received October 2008, revision accepted February 2009

ABSTRACT

Karst aquifers represent important but very vulnerable sources for water supply to a significant part of the Earth's population. For sustainable use of these resources, development of integrated management tools based on numerical groundwater models is required. In principle karst aquifers are characterized by the presence of two distinct flow domains: the limestone matrix fractures and the conduits. A flow model of karst aquifers requires detailed, spatially distributed information on the hydrologic characteristics of the aquifer and flow paths. Geophysical methods determining the distribution of the electrical resistivities within the subsurface could provide such information. An international scientific research project was initiated to explore the potential of airborne electromagnetic mapping for providing such innovative information for improving groundwater modelling of karst aquifers. The project study area is located in the Sian Ka'an Biosphere Reserve located in Yucatán, Mexico, a coastal wetland of international importance. As a first step ground geoelectric and ground electromagnetic measurements were performed in March 2006 to determine the electrical properties of the Sian Ka'an Biosphere Reserve subsurface environment. These results were used for 3D forward modelling to calculate the expected airborne electromagnetic response. Based on these promising results, an airborne pilot survey was performed in 2007 to evaluate the applicability of airborne electromagnetic methodology. This survey covers an area of 40 square kilometres above the well-mapped Ox Bel Ha cave system. The results showed that the signature of the cave system could be clearly detected. The pilot survey offered as well the chance to define the limits of current state-of-the-art airborne data acquisition and inversion. The study helped to define the needs for further developments and improvements to establish the frequency domain electromagnetic method as a practical karst exploration method.

INTRODUCTION

Karst terrain covers approximately 12% of the Earth's land surface and karst aquifers are important water resources in many parts of the world (e.g., Williams 1993; Ford and Williams 2007). Due to the rapid water flow in karst aquifers and their limited capacity for retention of pollutants, these water resources are extremely vulnerable to environmental pollution. Therefore, protection of karst areas is of major concern to ensure adequate water supply for a significant portion of the Earth's population (e.g., Darnault 2008).

In order to protect karstic groundwater systems and associated ecosystems, it is necessary to develop integrated tools for sustainable management of these resources based on accurate coupled surface-/groundwater models. Although the mathematical formulation of such models is well established, results are mostly unsatisfactory. The reason for this is that both location and geometry of dominant karst features, controlling the flow, are either not known at all or not known with the required accu-

* robert.supper@geologie.ac.at

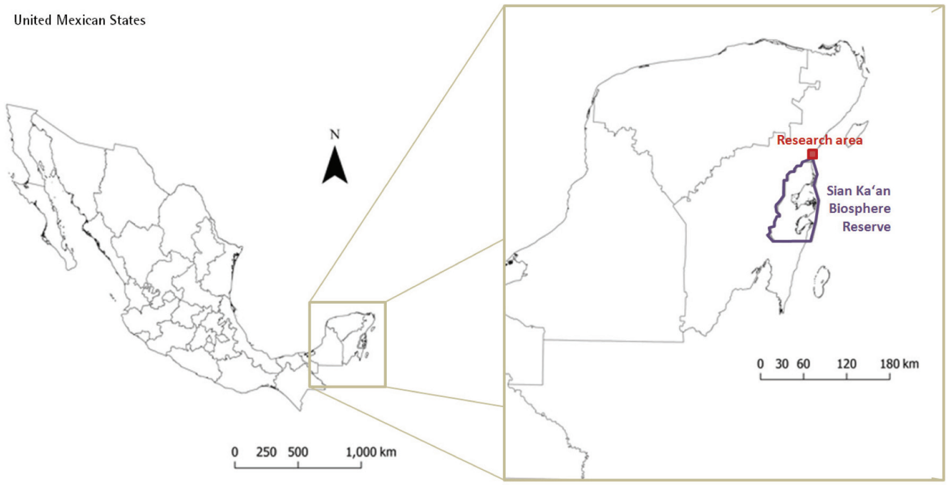

FIGURE 1
Location map of the SKBR and research area.

racy. Therefore, the results of hydrological modelling of karst aquifers could significantly advance if new and innovative technologies are developed to provide high-resolution constraints in groundwater models. The results of airborne electromagnetics could provide such information. The research project XPLORE was initiated to explore and improve the potential of airborne geophysical measurements and the associated interpretation techniques to provide such information.

The area around the Sian Ka'an Biosphere Reserve (SKBR) (for location see Fig. 1) was chosen as a test site as it offers favourable conditions for the application of the proposed frequency domain airborne electromagnetic techniques (FDEM) due to the following facts:

- The area is extremely flat and the karst is exposed right at the surface in the entire area, thus allowing low flight altitudes (60 m); almost no topographic effects are of concern.
- Topsoils are relatively thin and will not appreciably attenuate the electromagnetic signal.
- The dominant karst structures are located at shallow depth (max. 25 m).
- Though the karst conduit system in this area is largely unexplored, except in the Northern part, scuba diving for cave exploration has mapped the conduits. In this area the cave systems (e.g., Ox Bel Ha, Sac Actun) are known in great detail. The available cave maps can be used as ground truth for the interpretation of the airborne geophysical data.

These conditions form a perfect background for the evaluation of various technologies under simple boundary conditions.

First, ground geoelectric and electromagnetic measurements were applied to develop a general subsurface resistivity model for SKBR. Subsequently, forward modelling of frequency domain electromagnetic results using the above mentioned synthetic resistivity model was performed to evaluate the principal applicability of the methodology. Based on the promising results, a pilot airborne electromagnetic survey was conducted, covering an area north of the SKBR. The results of ground surveys, forward modelling and of the pilot airborne survey are presented here.

STATE-OF-THE-ART GEOPHYSICAL KARST EXPLORATION

Karstifiable rocks are a traditional focus of geophysical research (Bögli 1980). Several case studies can be found in the literature (e.g., McGath *et al.* 2002; Beck 2002; Cunningham 2002; Roth *et al.* 2002; Danbom 2005). Some successful results have been obtained using various geophysical methods, such as gravity (Debeglia and Dupont 2002), geoelectrics (Mingelli 1989; Zhou *et al.* 2002; Nyquist *et al.* 2007), coupled resistivity (Garmann and Purcell 2004), ground-penetrating radar (GPR) (Henson *et al.* 1997; Carreon-Freyre and Cerca 2006), proton magnetic resonance (Guérin and Benderitter 1995) and electromagnetics (Nyquist *et al.* 1999). On the Yucatán Peninsula, Steinich and Marin 1997 employed azimuthal resistivity surveys to identify directions of high permeability within the aquifer. Doolittle and Collins (1998) and Guerin and Benderitter (1995) demonstrated the application of two independent methods to improve the results of geophysical karst exploration.

As a shortcoming, all ground-based surveys are restricted by terrain accessibility. So far only a few studies are available where airborne geophysics has been applied to karst regions (Beard *et al.* 1994; Doll *et al.* 2000; Gamey *et al.* 2001, 2002; Mandell *et al.* 2003; Smith *et al.* 2003, 2005, 2008) we anticipate improvement for karst exploration results using airborne multi-sensor (electromagnetic (EM), very low frequency (VLF), Gamma) surveys, although their potential has not yet been explored exhaustively. Finally, two papers by Bosch and Müller (2001, 2005) suggested VLF gradient surveys for innovative high-resolution surveys over vulnerable karst regions. Most of these studies have focused on structural investigation and basement mapping in karst areas. However, the authors do not know of any study where results derived from airborne geophysical data have been used to characterize hydrological units for the modelling of karst aquifers.

To conclude, geophysics has shown that ground-based methods can identify aquifer units on a local basis. The ground-based data collection is only local and time- consuming and it is not realistic to apply it to the exploration of large groundwater systems, especially in inaccessible terrain. Airborne multi sensor platforms can be applied over large areas to map hydrostratigraphic units. However, results so far from airborne data have not been related to the characteristics of aquifer units. On a regional scale the role of geophysics and especially of remotely sensed data, has definitely not been fully exploited.

THE RESEARCH AREA

The Sian Ka'an Biosphere Reserve (SKBR), located on the Yucatán Peninsula, Mexico (Fig. 1), is a UNESCO World Heritage site, established in 1986. It is composed of a number of different ecosystems. The marine area of the SKBR includes parts of the widespread barrier reef system along the eastern coast of Central America (Morales 1993). The terrestrial ecosystems encompass evergreen and deciduous forests, savannahs, freshwater and saltwater marshes, mangroves and dunes (Morales 1992, 1995; see Fig. 2). The rainforests are part of the Gran Selva Maya, which is the world's largest continuous rainforest area north of the Amazon Basin. The reserve is home to a wide variety of wildlife including puma and jaguar and it hosts dozens of colonial water bird species.

SKBR is primarily fed by subsurface flow through the karstified limestone of the Yucatán plain. The general groundwater flow pattern on the Yucatán Peninsula is generally believed to be characterized by a radial flow pattern from the centre of the peninsula towards the coasts at the peninsula margins. However, locally, flow directions can be highly variable depending on the orientation of karst conduits and fractures.

The area receives precipitation of around 1000 to 1500 mm/year. Evapotranspiration is not well determined but estimates range between 40% (Beddows 2004) to 85% (Lesser 1976) of mean annual precipitation.

The underground hydrologic system in the study area is the key ecological link between the tropical forest, wetlands, coral reef and other marine ecosystems, as well as the human activities associated with those environments. Pressure on the reserve has been increasing over the years due to accelerated tourism development in the region, increased domestic water demand, contamination with agricultural fertilizers and pesticides as well as infrastructure projects, illegal hunting activities and extensive fishing. High population growth rates (over 10% per year in the region), high tourism activity (about 10 million visitors to the region in 2004) and poor waste water treatment (less than 30% of the total waste water produced in the region is treated in any way), makes water quality issues one of the area's most important and significant social and environmental problems and demands an integrated approach towards the management of SKBR.

On a local scale, the municipality of Tulum, located a few kilometres north of SKBR, is currently in the process of designing an urban development plan (Programa de Desarrollo Urbano del Centro de Población de Tulum (PDU), Gaceta Parlamentaria, (http://gaceta.diputados.gob.mx/Gaceta/60/2008/abr/20080430.html), año XI, número 2496, miércoles 30 de abril de 2008). The preliminary version of the PDU promotes the establishment of 60 000 hotel beds in Tulum. Presently Tulum has about 12 000 inhabitants and the PDU foresees an at least tenfold increase in the local population. The urban area is expected to expand significantly reaching the border of the SKBR in the south.

At the moment, knowledge on the hydrogeology of the area discussed in the PDU is fragmentary. Cave divers have explored parts of the karst conduits but up to date no systematic study on aquifer geometries and properties, groundwater flow directions and velocities exist. Two major problems are associated with the unknown aquifer structure in the area of the PDU: i) large karst cavities can collapse and are a potential hazard for the planned hotels and infrastructure in the area and ii) large quantities of wastewater will be generated by the increased permanent population and the visitors. A coherent concept for the treatment and disposal of the wastewater is lacking (Beddows *et al.* 2007;

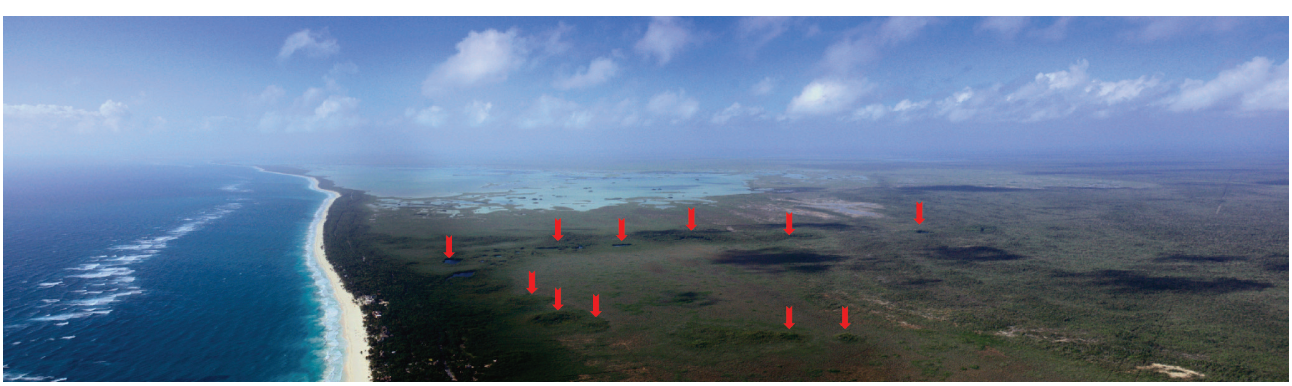

FIGURE 2

Airborne photograph showing part of the SKBR (photography: R. Supper, 02-2008; panorama stitching: A. Ahl) showing the different ecosystems: left side: Caribbean Sea with barrier reef and dunes, central back side: saltwater and freshwater lagoons, central foreground: mangrove woods and savannah, right side: rainforests of the Gran Selva Maya; in the central area, several cenotes can be recognized (red arrows), whose alignment marks the course of the main subsurface cave system.

Amigos de Sian Ka'an, Resultados de la Reunión. Document from the CD-Rom of the workshop: Construyendo las Bases Para la Conservación del Agua y su Biodiversidad Asociada en la Península de Yucatan. 10 y 11 de noviembre 2003, Cancún Quintana Roo Amigos de Sian Ka'an, The Nature Conservancy y la Comisión de Áreas Naturales Protegidas.; Krekeler *et al.* 2007). Local authorities favour re-injection of the wastewater into the deeper aquifer units, beneath the halocline (Beddows *et al.* 2007; Sam Mecham (pers. comm.) with the cave diver and director of Centro Investigador del Sistema Acquífero de Quintana Roo A.C. (CINDAQ) April 2006). However, due to its lower density compared to seawater, the wastewater may potentially resurface and pollute the freshwater lens that is currently serving as the backbone for water supply to the region. Wastewater discharge into the ocean will in turn endanger the ecological integrity of the coral reef, which is one of the prime economic assets of the region. Finally, it is presently unknown, whether some of the large subsurface conduits connect the area of the PDU to SKBR and whether the hydraulic gradient is directed towards or away from the reserve. In order to develop sustainable options for wastewater disposal and enhanced urban development of Tulum, an aquifer characterization and modelling study is urgently required.

GEOPHYSICAL KARST EXPLORATION RESULTS FOR THE SKBR

The application of airborne electromagnetic methods to map large-scale karst systems over wide-ranging areas seems promising to aid the above studies. However, karst conduits can only be detected by this method if the contrast between the resistivity of the carbonate host rock and the resistivity of the karst features is sufficiently high. Consequently, to start an airborne survey in Mexico without any preknowledge would pose a high financial and logistical risk. Therefore, a pilot ground based resistivity survey was performed in March 2006 to determine the electrical properties of

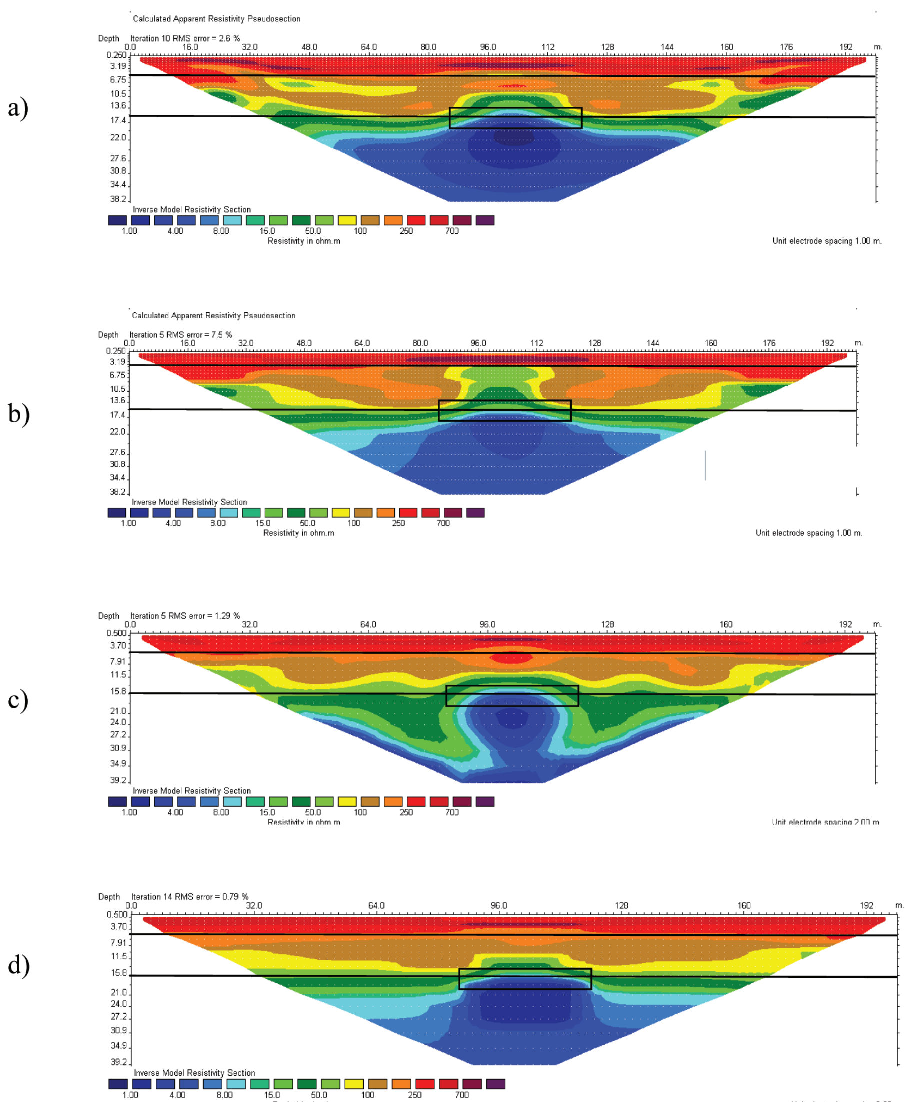

FIGURE 3
Results of inversion of synthetic geoelectrical data (Schlumberger configuration) with RES2DINV using different settings: a) smooth inversion, model block spacing: half electrode distance; b) robust inversion, model block spacing: half electrode distance; c) smooth inversion, model block spacing: unit electrode distance; d) robust inversion, model block spacing: unit electrode distance; black lines and rectangle indicate the shape of the initial model.

the SKBR subsurface environment. Subsequent forward modelling was applied to evaluate the potential success of applying airborne electromagnetic methods to map large-scale karst features within SKBR. On the other hand the inversion results gave important ground truth for the interpretation of the airborne electromagnetic field data from the airborne pilot survey.

The ground-based geoelectric survey campaign

Geoelectric multielectrode measurements and ground based electromagnetic (EM-34) profiles have been the method of choice to derive high-resolution 2D models of the subsurface resistivity structure, including cave systems, known from scuba diving exploration (based on the unpublished cave maps supplied by Sam Mecham (CINDAQ) and Robbie Schmittner (Xibalba Dive Center) (pers. comm.), for names of individual cave explorers see acknowledgements) at different locations.

Results of forward modelling and inversion of synthetic geoelectric data

Due to ambiguities inherent to the geoelectrical method, it is unlikely that the exact shape of a cave could be recovered from inversion of field data. However, the inversion could be improved by applying constrained inversion parameters. Based on a synthetic subsurface model, a geoelectric pseudosection was calculated for the Schlumberger configuration and subsequently inverted using different inversion parameters. The cave model used was set up according to the results of direct conductivity measurements over the cave system and field inspections performed during the first days of the field survey. The parameters were defined for a typical subsurface setting approximately 6–8 km inland from the Caribbean Sea. The average groundwater table at that location was found at a depth of 4.5 m, the depth to the halocline (interface between brackish (4 Ohmm) and marine (0.2 Ohmm) water) at 16 m. The cave was assumed to be located between a depth of 14 m and 20 m and to exhibit a width of 34 m (located between profile distance 86 m and 120 m). A bulk resistivity value of 500 Ohmm was assigned to dry limestone, 100 Ohmm to saturated limestone filled with brackish water and 6 Ohmm to saturated limestone with saline water filling. Subsequently the calculated values have been inverted using the RES2DINV (Loke and Dahlin 2002) and EarthImager 2D (http://www.agiusa.com/agi2dimg.shtml) software. Figure 3 presents the results for the RES2DINV software inversion using a) smooth, b) robust inversion based on model cells with width of half the unit electrode spacing (herein after referred to as ‘smooth / robust half distance’) and c) smooth, d) robust inversion based on model cells with a width of one unit electrode spacing (herein after referred to as ‘smooth / robust normal distance’). The results showed that in all cases the horizontal location of the cave was reconstructed quite well whereas the exact geometry and depth below surface of the initial model could not be resolved. The depth to the top of the cave was generally underestimated (5–10 m). The depth to the bottom of the cave (27–30 m) as well as the actual resistivity of the brackish (15–50 Ohmm) and

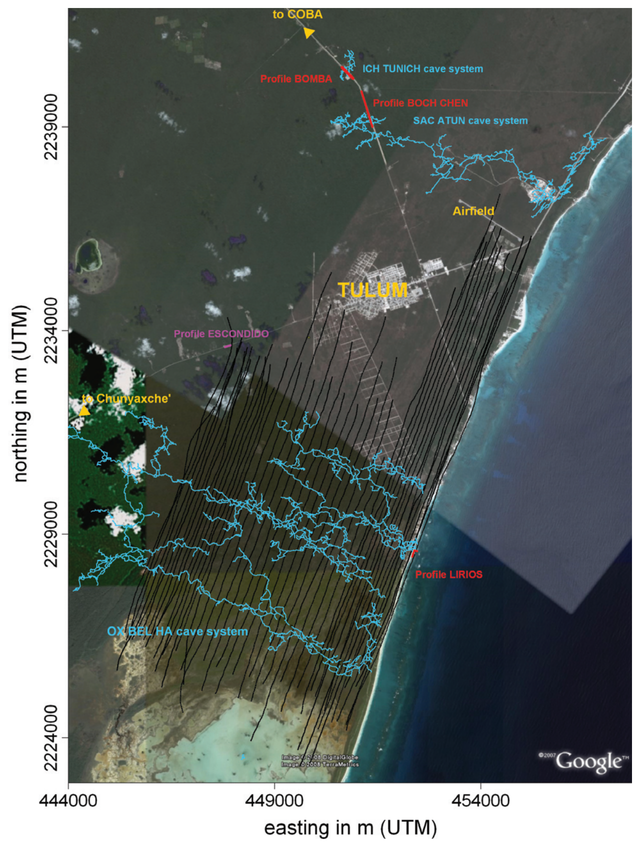

FIGURE 4
Location map showing the mapped cave systems (blue), geoelectrical profiles (red), the electromagnetic ground profile (purple) and airborne electromagnetic profiles (black). In the background, a satellite image taken from ‘Google Earth’ is shown.

saline portion (1–4 Ohmm) of the cave, was overestimated. In the ‘smooth half distance’ case 3a) an intermediate low resistivity layer on either side of the cave at an average depth of 7 m was introduced. The best indication for the presence of a cave could be derived in the ‘robust half distance’ case 3b), whereas the most realistic representation of the input model could be obtained using the ‘robust normal distance’ d) parameter set. Results for the Earth Imager software show similar results, although edge effects are much smaller.

The experience gained from these modelling studies, together with geological background information, was used to select inversion parameters and constraints for the inversion of the actual field data.

Results of geoelectric field measurements

Based on the results from scuba diving exploration several profiles were selected crossing known karst caves at different subsurface conditions. As most of the area is covered by dense vegetation, only a few locations over known cave systems were actually accessible to perform ground surveys. The locations of the measured profiles are indicated in Fig. 4. For this paper three profiles were selected as they investigate the subsurface resistivity structure at different constraints. The profile near Cenote Bomba investigates the near surface response from a well-known cave branch at 8 km distance from the sea whereas profile Cenote Boch Chen is intended to survey resistivities within the deeper subsurface below the halocline. Profile Lirios examines the typical subsurface resistivity pattern nearby the coastline.

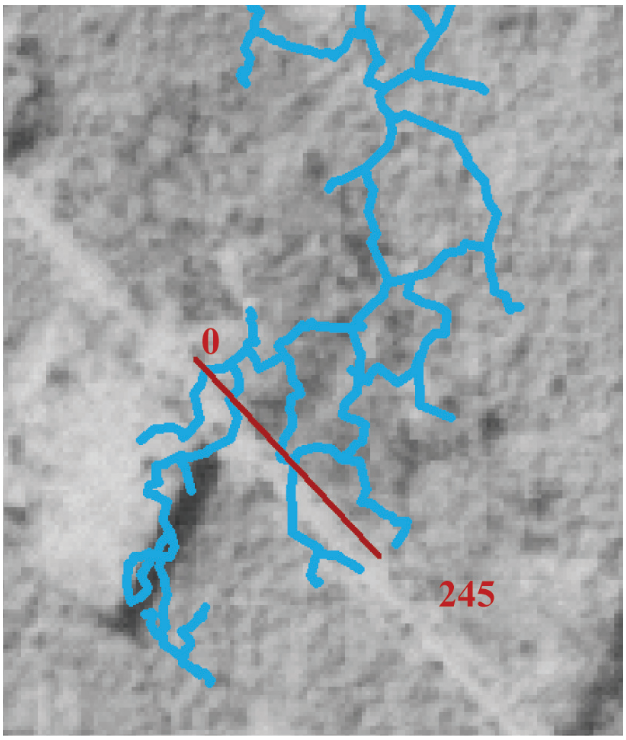

FIGURE 5
Location of the geoelectrical profile BOMBA in relation to the subsurface cave system, mapped by cave diving exploration (red line: geoelectric profile Bomba; light blue lines: mapped line inside cave system).

Profile Cenote Bomba

This profile was measured in an area 4–5 km north of Tulum, parallel to the main street to Coba between the two cenotes (Mexican word for sinkhole) 'Bomba' and 'High Voltage'. According to the scuba divers' exploration a large cave crosses the profile right in the middle (see Fig. 5, crossing point between profile distance 110 m and 150 m). The bottom of the cave could be expected at a depth of 16 m. Figure 6 shows the results of inversion for a) the Res2dinv (robust, half unit spacing) and for b) the EarthImager (smooth inversion, average resistivity of pseudosection was used as starting model) software. In both inversion results the existence of a cave could be detected quite clearly in the middle part of the section. The depth to the groundwater table was located at a depth of 5 m below ground level (bgl). The resistivity of the fresh/brackish groundwater layer was found to be relatively high (>150 Ohmm), suggesting a low porosity of the un-karstified limestone. The halocline is detected quite clearly as a resistivity gradient, although its depth (approximately 18 m) is overestimated by Earth Imager (25 m). The latter smooth inversion also detects three more caves at 33 m, 66 m and after 216 m along the profile, which can be correlated with caves known from the cave map. The similarity of the result shown in Fig. 6(a) with the forward modelling result of Fig. 3(b) is obvious. However, the result of the smooth inversion of Fig. 6(b) seems to enhance small variations in the measured resistances, eventually due to noise potentials, thus producing resistivity pattern with unrealistically high resolution.

Profile Cenote Boch Chen

This profile was measured near profile Bomba on the highway to Coba, starting near Gran Cenote and crossing the side tunnels of Cenote Boch Chen in the middle part of the profile between 300 m and 400 m. This profile was carried out to investigate the resistivity distribution at greater depths (>140 m). To reach these depths an electrode spacing of 10 m was used. Due to this large

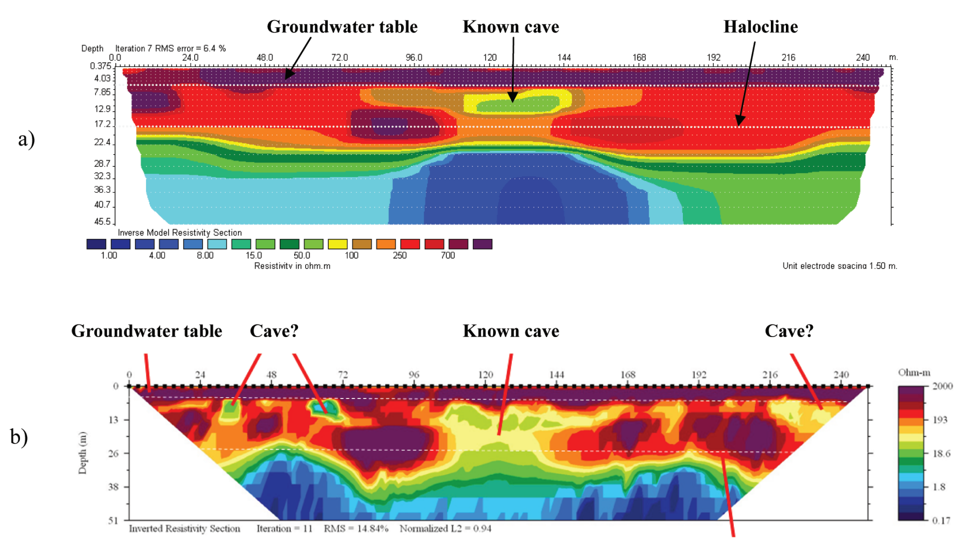

FIGURE 6
Results of inversion of geoelectrical data (Schlumberger-Wenner configuration) on profile Bomba: a) RES2DINV robust inversion, model block spacing: half electrode distance; b) EarthImager smooth inversion, starting model: average apparent resistivity.

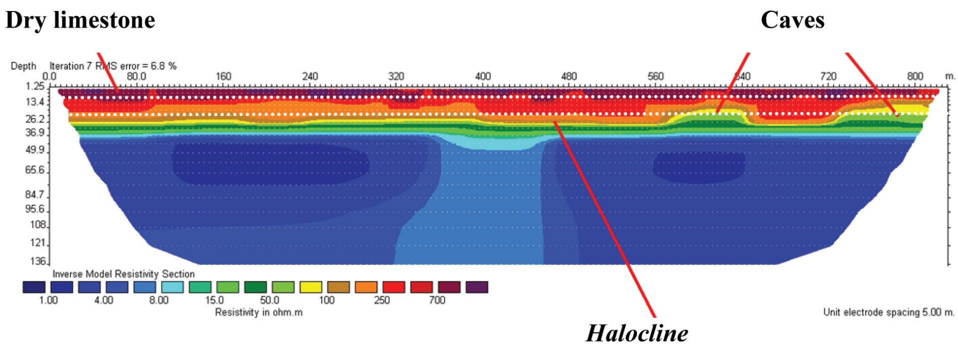

FIGURE 7
Results of inversion of geoelectrical data (Schlumberger-Wenner configuration) on profile Cenote Boch Chen: RES2DINV robust inversion, model block spacing: half electrode distance.

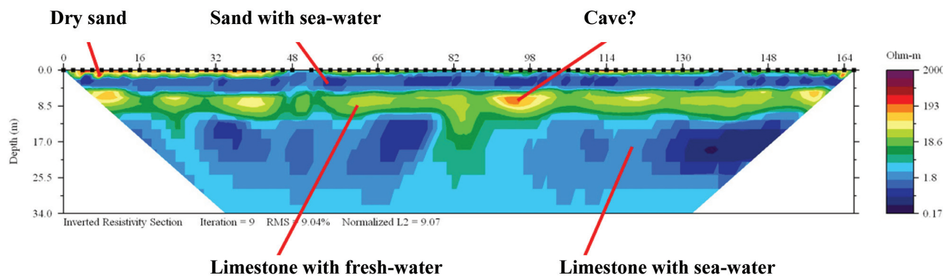

FIGURE 8
Results of inversion of geoelectrical data (Schlumberger-Wenner configuration) on profile Lirios: EarthImager robust inversion, starting model: average apparent resistivity.

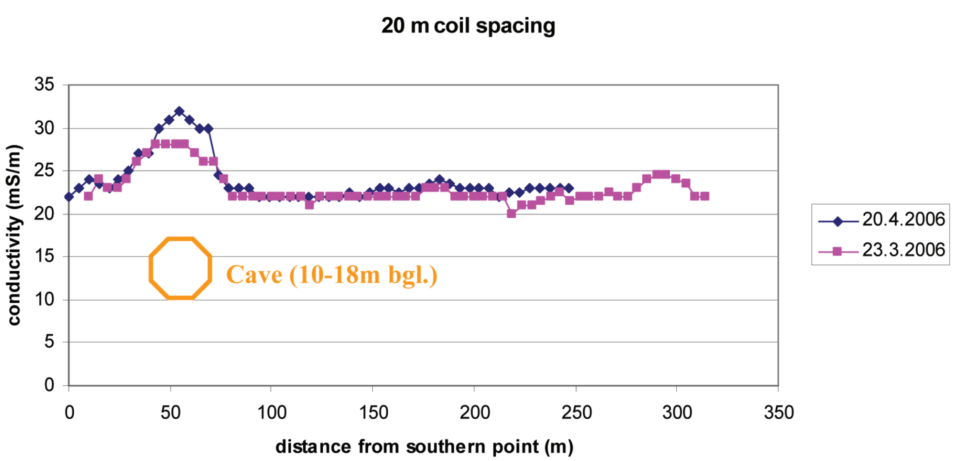

FIGURE 9
Results of EM-34 profiling (coil separation 20 m, frequency 1.6 kHz) over a known cave branch between cenote Cristal and cenote Escondido (apparent conductivities given).

electrode spacing no details about the shallow cave system could be expected. The data was inverted with a model block size of half the electrode spacing.

Figure 7 shows the result of the robust inversion. The high resistivity surface layer with values above 700 Ohmm suggests a thickness of almost 5–7 metres, corresponding well with the measured groundwater table in cenote Boch Chen at around 5 m bgl. Despite the large electrode spacing and therefore low resolution at near surface, several anomalies could be detected in the medium resistivity layer. The crossing of the known caves between 300 m and 320 m as well as between 345 m and 400 m are not very clearly seen although a slight decrease of resistivities is visible. Lower anomalies between 600–640 m and beyond 740 m suggest the existence of two caves but no scuba diving data is available yet.

From 21–31 m downwards we find a successive decrease of resistivities from 200–4 Ohmm. This transition zone corresponds to one model block thickness and might be an artefact of the inversion process, which is not able to reproduce such large and abrupt resistivity contrasts. Therefore, the depth of the halocline has to be fixed at around 21 m, which again corresponds well with the field and scuba diving observations. Below the halocline hardly any structures can be found except an increase in the middle part of the profile and a smooth increase with depth. No interpretation could be derived from the inversion results of the deeper parts, as the data for the field measurements were very noisy due to the nearby transformer station.

Profile Lirios

This profile was measured in the coastal area along the beach to investigate the resistivity distribution in an environment with a very thin freshwater aquifer. Here, brackish water filled caves, embedded in seawater filled background formations are expected. At greater depths seawater filled caves should be found. The results of the inversion (Fig. 8) show a thin, high resistivity top layer, correlating with dry beach sands. The groundwater table was found at 1.15 m below surface. Below, seawater filled dune-sands can be found, showing resistivities below 1 Ohmm and a thickness of 4–5 m. From 5–10 m depth, higher resistivity values between 5–200 Ohmm were detected, underlain by values below 2 Ohmm. A possible interpretation of the higher resistivity layer is that near the coastline, shallow karst areas are filled with brackish water, both in voids/caves (higher resistivity) whereas in the surrounding matrix (lower resistivity) salinity is higher due to mixing processes. However, interpretation is very difficult due to the ambiguities of the resistivity versus porosity/salinity relationship. In the deep low resistive layer, some extremely low resistivity anomalies can be estimated perhaps suggesting cave systems. We can conclude that due to the very low resistivities near to surface, most of the current is expected to be channelled within this layer. Consequently only some principal qualitative information about the resistivity structure below can be derived from geoelectric measurements, whereas quantitative conclusions on depths and thicknesses are very approximate.

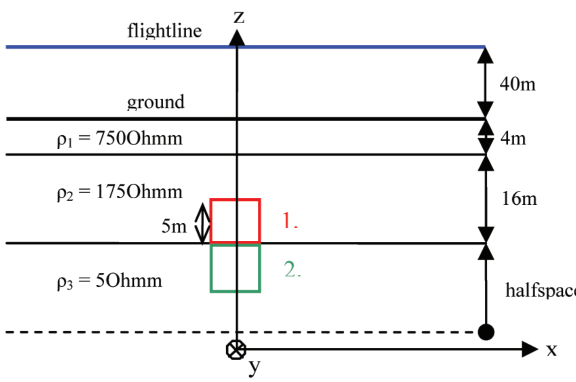

FIGURE 10
Cross-section of the model used for forward modelling, model case: deep situated halocline, cave located 1) inside limestone, saturated with brackish water (5 Ohmm) and 2) inside limestone, saturated with saline water (0.2 Ohmm), first layer: dry limestone.

Results of ground electromagnetic field measurements

Electromagnetic measurements using the Geonics EM-34 equipment were originally planned parallel to all geoelectric profiles. However, in most cases power lines were present in the vicinity of the profiles that produced a high noise level prohibiting reliable measurements. Only measurements along the profile Escondido, situated (see Fig. 4) along the highway Mex 307

TABLE 1
Specification of the Austrian airborne system

	Frequency (Hz)	a (m)	Configuration
Frequency 1 (f1)	340	4.53	Vertical-coplanar
Frequency 2 (f2)	3200	4.53	Horizontal-coaxial
Frequency 3 (f3)	7190	4.49	Vertical-coplanar
Frequency 4 (f4)	28850	4.66	Horizontal-coaxial

a = separation between transmitter and receiver coil.

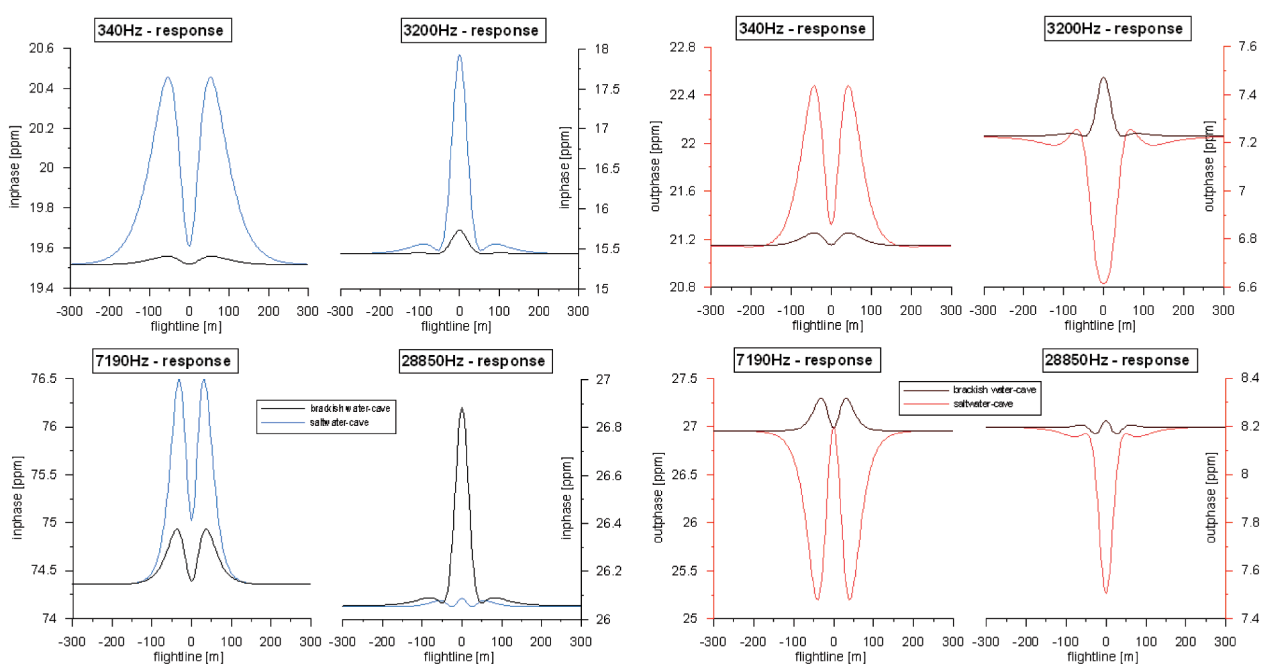

FIGURE 11
In-phase (black, blue) and out-of-phase (dark and light red) components calculated from the model of a brackish water- and saltwater-cave in case of a deep halocline.

between Chunyaxche' and Tulum, crossing one branch of the cave system connecting Cenote Naharon (Cristal) and Escondido (Mayan Blue) could be performed. Due to the heavy traffic on the road and limited space beside the highway, geoelectric measurements could not be carried out along this profile without endangering the field personal. The results (Fig. 9) show that a significant positive anomaly could be detected right above the cave. To prove reliability of the results, measurements along this profile were repeated one month later (blue curve), producing almost the same results.

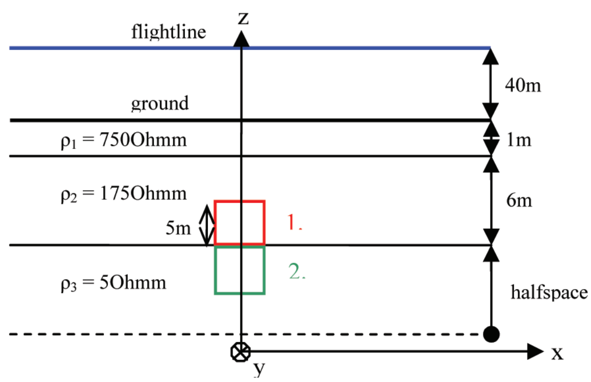

FIGURE 12

Cross-section of the model used for forward modelling, model case: shallow halocline, cave located 1) inside limestone, saturated with brackish water (5 Ohmm) and 2) inside limestone, saturated with saline water (0.2 Ohmm), first layer: dry limestone or dry sand.

The electrical model for the SKBR subsurface

The interpretation of geoelectric measurements showed that known caves in the research area could be detected by this technique. However, depth and size could be determined only very approximately. In the area near the coastline, where the brackish aquifer is very thin, no clear information about caves could be derived due to the ambiguity of the expected anomalies.

From a geoelectric point of view, the SKBR subsurface environment can be characterized as follows (see also Figs 10 and 12). Above the groundwater table, fractures and holes are mostly filled with air, thus representing a relatively high resistivity top layer (250–1000 Ohmm). Below, fractures are filled either with brackish (3–5 Ohmm) or saline (0.2 Ohmm) water. The halocline can be found at 4 m below ground level (bgl) nearby the sea (groundwater level 1 m bgl), dipping gently inland to a depth of approximately 20 m bgl at 7 km distance (groundwater level 6 m bgl). This corresponds well with halocline depths measured by Beddows (2004). The electrical resistivity of the saturated limestone matrix was determined to vary between 50–300 Ohmm (depending on actual porosity) above the halocline and 4–15 Ohmm below.

Due to these high resistivity contrasts, the applicability of an airborne frequency domain electromagnetic system, like the one operated by the Geological Survey of Austria (Motschka 2001), seemed very promising.

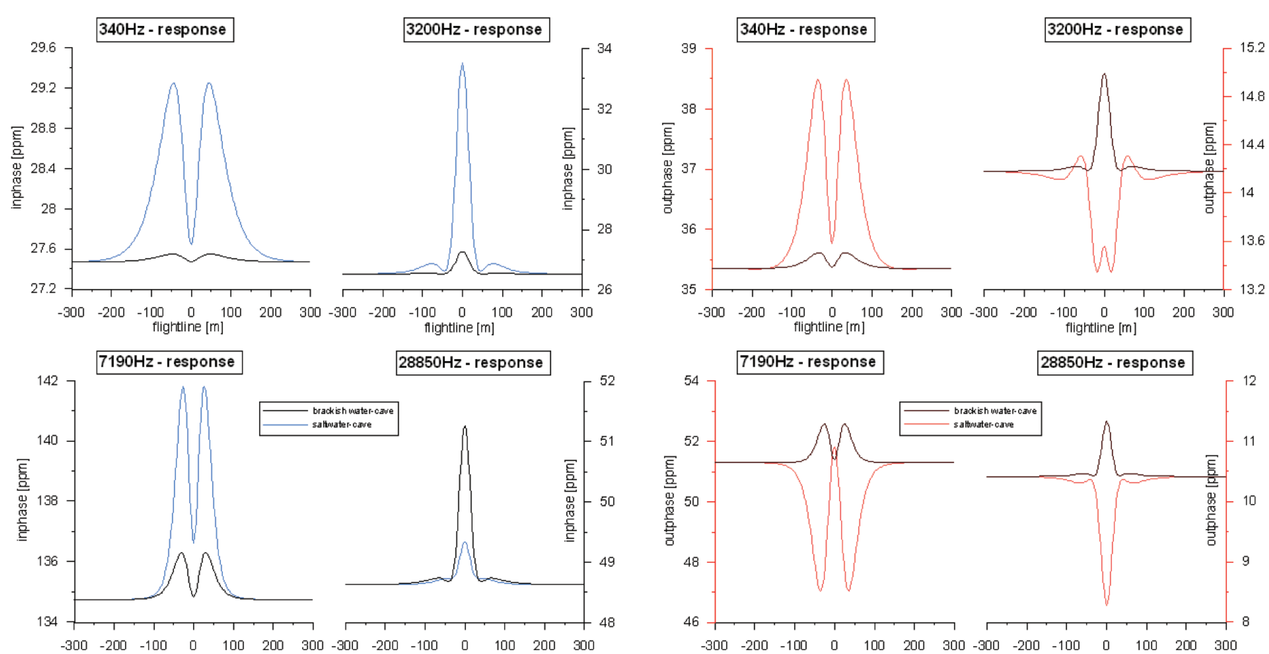

FIGURE 13

In-phase (black, blue) and out-of-phase (dark and light red) components calculated from the model of a brackish water- and saltwater-cave in case of a shallow halocline.

TABLE 2

Results of forward modelling, maximum amplitudes of anomalies in ppm for different EM-components are given for the different cases of forward modelling (shallow/deep/brackish-/saline-water filled cave), bold numbers indicate values above noise level and underlined numbers indicate highest anomaly amplitudes

	Shallow cave		Deep cave		Amplitude difference shallow/deep	
EM components	**Brack water**	**Saline water**	**Brack water**	**Saline water**	**Brack water**	**Saline water**
340Hz in-phase	0.1	**1.6**	0.1	**1**	0	0.6
340 Hz out-of-phase	0.25	**3**	0.2	**1.2**	0.05	**1.8**
3200 Hz in-phase	0.8	<u>7</u>	0.25	<u>2.5</u>	0.55	<u>4.5</u>
3200 Hz out-of-phase	0.8	0.8	0.3	0.6	0.5	0.2
7190 Hz in-phase	**1.2**	<u>7</u>	0.5	<u>2.2</u>	0.7	<u>4.5</u>
7190 Hz out-of-phase	**1.1**	**4**	0.3	**1.7**	0.8	**2.3**
28850 Hz in-phase	<u>2.7</u>	0.6	0.9	0.1	<u>1.6</u>	0.5
28850 Hz out-of-phase	0.8	**2.3**	0.02	0.7	0.75	**1.6**

All results are given in ppm.

THE AIRBORNE SURVEYING CAMPAIGN

Airborne electromagnetic forward modelling

To further evaluate the applicability of an airborne electromagnetic system for mapping karst features in the SKBR area, the theoretical response of a frequency domain airborne electromagnetic system (for system parameters see Table 1) over resistivity models derived from ground based geoelectric results (Figs 10 and 12) was calculated. Results for a large quantity of different model cases were calculated and analysed. For this paper we compare only cases highlighting the typical situation inside the investigation area of the pilot survey at two different distances (approximately 0.5 km and 8 km) from the sea. A rectangular cave (side length 5 m) was assumed to be located inside a limestone, saturated with brackish (red rectangle, case 1) or saline water (green rectangle, case 2). For details of the models, refer to Figs 10 and 12.

The software EMIGMA 7.5 (PetRos Eikon Inc.; Murray *et al.* 1999; Groom and Alvarez 2002) was used for the 3D-EM forward modelling. Results were verified using the AEM (version 2.2) software code developed by the AKP group (Avdeev *et al.* 1997, 1998; Pankratov *et al.* 1997). As results from both codes were basically identical, the outcome of the EMIGMA code was used for the figures of this paper.

Figures 11 and 13 show the results of forward modelling for the above models. The shape of the in-phase component anomaly clearly depends on the coil orientation: for horizontal-coaxial configuration the maximum of the anomaly is directly located above the centre of the cave. In case of vertical-coplanar arrangement a minimum marks the centre of the cave surrounded by two maxima. This is also valid for the shape of the 340 Hz out-of-phase component in vertical-coplanar orientation. For the other out-of-phase components, the shape is very much dependent on the depth and size of the caves. No general rules can be derived. For a good representation of the anomaly shape, different scales were used for the different components in Figs 11 and 13. To allow a comparison of absolute values, the results are summarized in Table 2. Black numbers indicate values above noise level and red and green bold numbers indicate highest anomaly amplitudes. The table clearly shows that the best response of a cave filled with saline water can be derived from the 3200 Hz and 7190 Hz in-phase components in case of a deep as well as a shallow cave. In both cases the maximum amplitude is far above the threshold defined by the general noise level (usually assumed around 1 ppm for the Austrian system). On the contrary a cave filled with brackish water can best be detected using the 28850 Hz in-phase component, although for the case of a deep situated cave the amplitude is at the edge of detectability.

The Austrian airborne system

Due to the promising results a pilot airborne survey was conducted in spring 2007 using the Austrian airborne electromagnetic (AEM) system. The main part of this system consists in a modified GEOTECH-'Bird' of 5.6 m length and 140 kg weight (Motschka 2001). It is towed on a cable 30 m below the helicopter. Inside the probe there are four transmitting coils as well as four receiving coils in different geometric arrangements (co-axial, coplanar loops; for details see Table 1). The transmitting coils generate an electromagnetic alternating field with frequencies of 340 Hz, 3200 Hz, 7190 Hz and 28850 Hz. This primary field induces eddy currents inside conductive subsurface layers. In turn the corresponding (secondary) magnetic field generated by these currents induces a current in the receiver coils. Based on the amplitude and the phase shift of the secondary field relatively to the primary field, conclusions can be drawn on the electrical resistivity of the subsurface. Variable frequencies and different geometric arrangements of the coils are used in order to allow depth-specific sounding of the subsurface. The lowest frequency determines the total penetration depth of the method (approximately 120 m below ground surface). The electromagnetic bird was supplemented by a

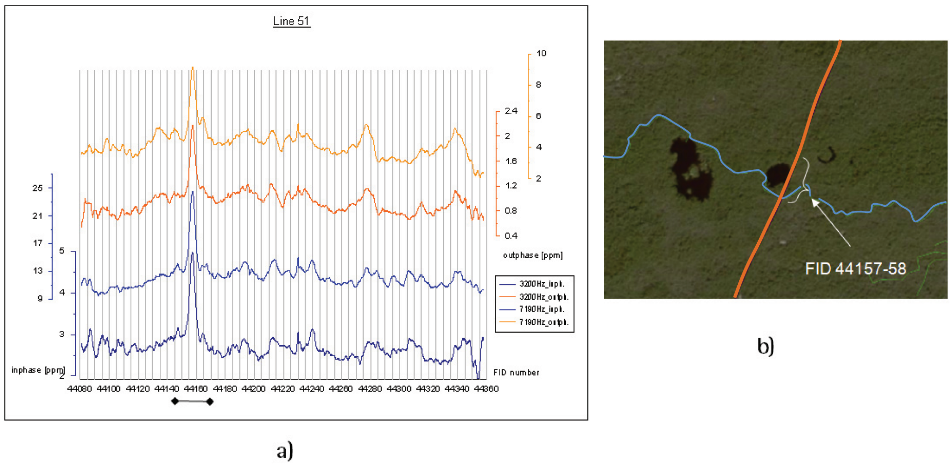

FIGURE 14
a) Results of drift corrected raw data (3200/7190 Hz in-phase (blue) and out-of-phase (orange)) over a known cave system (line 51, at 3.5–3.9 km distance to the coast) and a cenote; b) satellite image, showing several cenotes (black areas) inside the rain forest; location of mapped cave system (blue line) and flight path of survey helicopter (orange line) are overlain. Between fiducials 44157 and 44158 a significant anomaly due to the caves/cenotes influence can be detected.

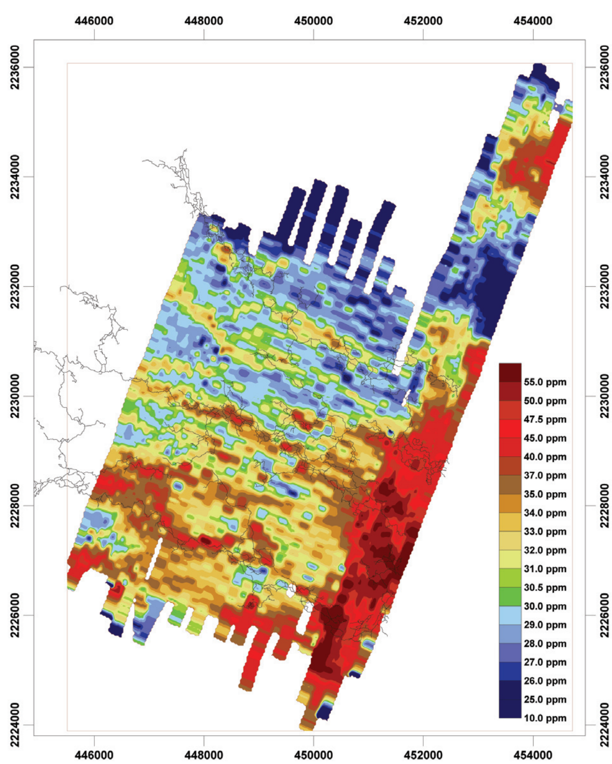

FIGURE 15
Results of the in-phase component of 7190 Hz after rough empirical altitude correction and profile levelling, colour bar chosen to highlight high- and low-amplitude areas; structure of known caves (black lines) are overlain.

laser altimeter and 2 differential GPS sensors, one located in the bird and one in the helicopter and a Cs-magnetometer. Additionally, gamma spectroscopy was applied.

The field survey

The pilot survey was carried out in April 2007 after half a year of intensive logistical preparations. An investigation area of almost 80 square kilometres (see Fig. 4) was selected between the town of Tulum and the lagoons of the SKBR (Fig. 2), partly covering the Ox Bel Ha cave system, which has been extensively mapped by cave divers. This area was covered with regularly spaced flight lines (for location of the flight lines see Fig. 4) at a separation of 100 m. In the middle part of the area a line spacing of 200 m had to be used due to limitations in available helicopter time. The target operating altitude of the helicopter was 70 m above ground surface, corresponding to a sensor altitude of 40 m. The distance between helicopter and ground surface was measured by a RIEGL LD90-3300HR laser-altimeter. The ground-distance of the helicopter was collected at a rate of 100 times per second. However, a laser ray is not only reflected from the ground surface but also from vegetation and manmade objects (for example buildings). Therefore, delicate processing algorithms had to be applied to compensate for this undesired effect. Basically, the maximum reflection times of all recordings within a time window of 0.1 second along the profile were calculated and converted to distances between helicopter and ground surface. Based on these results and considering the length of the bird-cable and sensor displacements due to the speed of the helicopter, the distance between the bird and the ground surface was calculated.

As a first processing step, thermal drifts in each of the measured components (in-phase and out-of-phase components of all frequencies) were removed from the AEM-raw-data. Such drifts are long-term variations of the measured signal not caused by geological sources. Furthermore, parts of the AEM signal, which were disturbed by manmade noise (i.e., by power lines, electric motors, transformers) were removed.

Figure 14 shows one example of drift corrected measurements over a known sinkhole (cenote). Around fiducial number 44158, directly above the location of a cenote, a significant positive anomaly was recorded. Although the influence of variations in flight altitude is still inherent in the drift corrected data, altitude variations were not the cause for the detected EM anomaly in this case.

To derive a consistent picture of anomaly pattern for the detection of caves an empirical altitude correction and subsequent profile levelling (similar to the methodology of Huang (2008)) was applied to roughly compensate for variations in flight altitude. It has to be stated clearly that this algorithm was only used to enhance the pattern of the phase components with the goal to map the location of the caves. No further inversion can be applied on the resulting data. Figure 15 shows the results for the 7190 Hz in-phase component, overlain with the known cave system (black lines). Clearly a large quantity of linear structures can be delineated, which correlate with most of the well-mapped cave systems. Anomaly alignments in the 7190 Hz in-phase component suggest the existence of several other, so far unexplored, branches of the cave system. Within recent months, cave divers have already verified some of these new structures (R. Schmittner 2008, pers. comm.).

Finally the drift corrected AEM data were inverted assuming a homogeneous half-space as subsurface model. In this kind of inversion the electric resistivity of a homogeneous, laterally and downward infinitely expanded half-space is calculated for each single data point. This 'apparent' resistivity is calculated from the bird altitude plus one single component or any combination of AEM components. To obtain a lateral resistivity distribution, the resistivities of all of these 1D models are stitched together (Sengpiel and Siemon 1998; Zhang *et al.* 2000). In contrast to the recorded AEM components, the calculated resistivities should be independent of the sensor altitude. Therefore, variations in bird altitude no longer influence the derived anomaly pattern. A water (salt-water, fresh-water or brackish water) filled cave surrounded by a saturated limestone matrix, should then be highlighted as a low resistivity anomaly.

Based on the results from forward modelling (Table 2) distinct components and combination of components were selected as input parameter for inversion.

As known from forward modelling, the homogeneous half-space resistivity, calculated from the in-phase component of the 28850 Hz frequency and the bird altitude, mainly maps the surface karst layers (dry limestone or limestone saturated with brackish water) and caves filled with brackish water in most of the survey area (see Fig. 16). Due to the low penetration depth, only shallow caves can be seen. Especially in the NW part of the survey area, directly SSW of the town of Tulum, the rise of the topography additionally causes an increasing distance to the water level, indicated by high resistivities above 60 Ohmm in the results derived from the 28850 Hz in-phase signal.

Along the coastline and in the region of the lagoons remarkable low resistivity areas can be seen. These anomalies are most likely caused by near surface seawater intrusions along the coast (verified by the results from the geoelectric profile Lirios

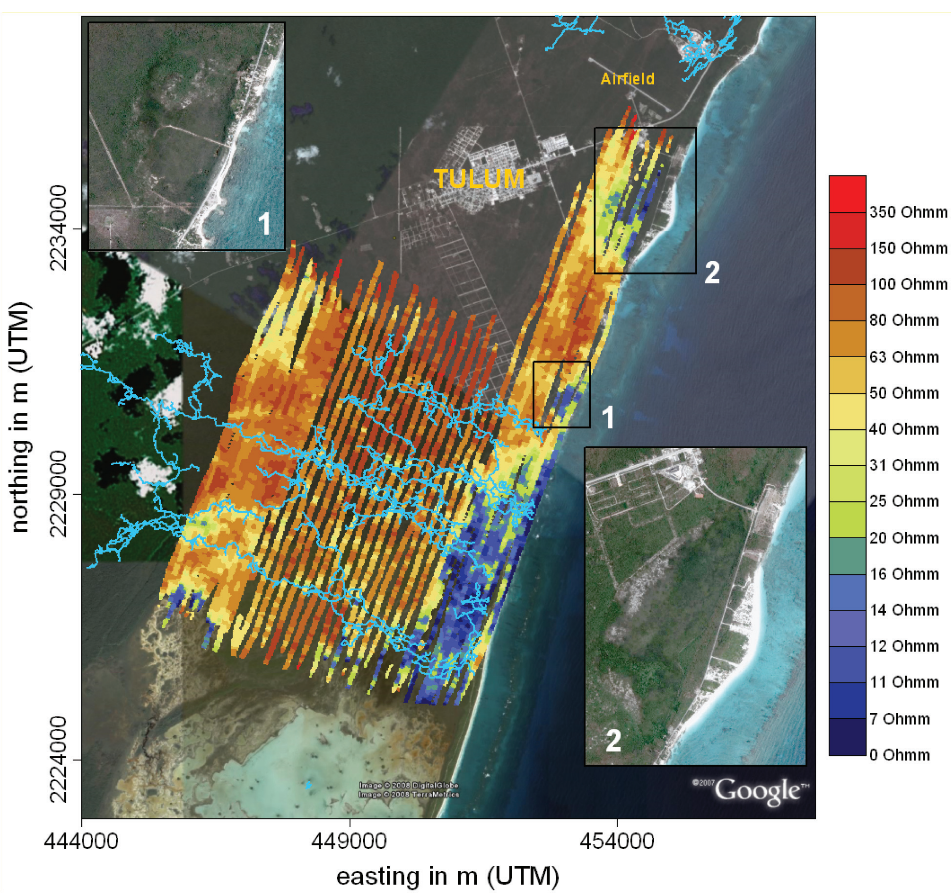

FIGURE 16
Homogeneous half-space calculated from in-phase component of the 28850 Hz frequency and the bird altitude. As an overlay, cave systems mapped by scuba-divers (light blue lines) are shown.

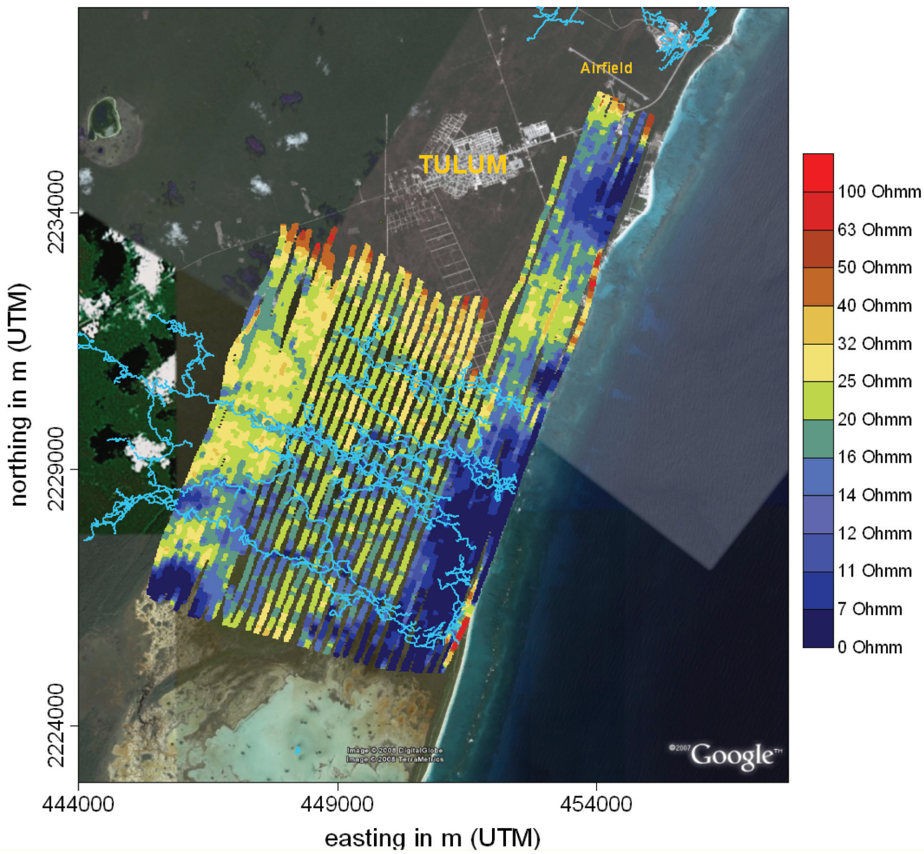

FIGURE 17
Results of homogeneous half-space inversion calculated from in-phase component of 3200 Hz and 7190 Hz frequency and the bird altitude. As an overlay, cave systems mapped by scuba-divers (light blue lines) are shown.

(Fig. 8)) or brackish water at the surface (in the area of the lagoon). The areas of low resistivity along the coastline in the northern part of the survey area are highlighted also by a visible change in vegetation (see satellite image as inlet to Fig. 16).

A good representation of the cave system is shown in the pattern of the half-space resistivities derived from the in-phase component of the 3200 Hz and 7190 Hz frequency (Fig. 17).

This behaviour was predicted by model calculations. In Figs 16 and 17 the caves can be seen as low resistivity anomalies. Anomalies aligned along the direction of the flight lines (SSW-NNE, Fig. 4) are mainly caused by non-linear drift components, which could not be corrected properly in the individual AEM components. These anomalies are particularly observed in areas flown with a line spacing of 200 m. This result emphasizes the need of a line spacing of not more than 100 m for such investigations and good drift/altitude correction.

CONCLUSIONS

The ability of airborne frequency domain EM measurements to localize and map karstic cave systems was demonstrated. For the investigated area the derived results could be verified by the available cave maps constructed by cave divers. Additionally, some previously unknown branches of the cave system were detected, of which some have recently been verified by divers guided by the prospective maps derived from the electromagnetic results. However, the results represent only a first step towards the definition of hydrological subsurface units. Inspection of the raw data and forward modelling indicate that additional information on the depth of the halocline, the resistivity of the limestone matrix and probably on the size and depth of the caves could be derived. To extract all inherent information from the field data multi-layer inversion algorithms constrained by boundary conditions have to be applied to make all information usable for advanced groundwater modelling. Additionally, the results have to be calibrated by ground measurements and borehole logs to better understand the relation between resistivity and matrix porosity of karst systems in order to allow proper interpretation of the results.

ACKNOWLEDGEMENTS

This survey was financially supported by the Austria Science Fund in frame of the project L524-N10 ‘XPLORE’ and by ETH Zurich. We further acknowledge financial support by The Nature Conservancy, the Technical University of Denmark, the COWI Foundation, the WWF Verdensnaturfonden/Aase & Ejnar Danielsens Fond 2006 and 2007 and UNESCO. We would like to sincerely acknowledge the support of Sam Meacham, Centro Investigador del Sistema Acuífero de Quintana Roo (CINDAQ), Martin Heidovitsch, Joyce Coleman, Robbie Schmittner, Xibalba Dive Centre, Mario Rebolledo Vieyra, Centro de Investigación Científica de Yucatan (CICY), A.S. Gutierrez of NAFTA for importing and exporting the scientific equipment, Caribbean Air and Global Vision International Mexico.

We are very grateful to Grupo de Exploraction Ox Bel Ha for permission to use the Ox Bel Ha cave line maps. Line maps kindly provided by Quintana Roo Speleological Survey 2006. Principal explorers of the Ox Bel Ha system: B. Birnbach, S. Bogaerts, F. Devos, C. Le Maillot, S. Meacham, B. Philips, S. Richards, D. Riordan, S. Schnittger, G. Walten and K. Walten. We would like to thank Bruce D. Smith and Richard Smith for reviewing the paper. Their valuable suggestions and comments significantly improved the quality of the paper.

REFERENCES

Avdeev D.B., Kuvshinov A.V., Pankratov O.V. and Newman G.A., 1997. High-performance three-dimensional using modified Neumann series. Wide-band numerical solution and examples. *Journal of Geomagnetism and Geoelectricity* **49**, 1519–1539.

Avdeev D.B., Kuvshinov A.V., Pankratov O.V. and Newman G.A. 1998. Three-dimensional frequency domain modelling of airborne electromagnetic responses. *Exploration Geophysics* **29**, 111–119.

Beard L.P., Nyquist J.E. and Carpenter P.J. 1994. Detection of karst structures using airborne EM and VLF. 64th SEG meeting, Los Angeles, California, USA, Expanded Abstracts, 555–558.

Beck B. 2002. The karst conferences, consulting reports as science, and geophysical pitfalls. *Engineering Geology* **65**, 81–83.

Beddows P.A. 2004. *Groundwater hydrology of a coastal conduit carbonate aquifer: Caribbean coast of the Yucatán Peninsula, México*. PhD thesis. School of Geographical Sciences, University of Bristol.

Beddows P.A., Smart P.L., Whitaker F.F and Smith L.S. 2007. Decoupled fresh-saline groundwater circulation of a coastal carbonate aquifer: Spatial patterns of temperature and specific electrical conductivity. *Journal of Hydrology* **346**, 18–32.

Bögli A. 1980. *Karst Hydrology and Physical Speleology*. Springer.

Bosch F. and Müller I. 2001. Continuous gradient VLF measurements: a new possibility for high resolution mapping of karst structures. *First Break* **19**, 343–349.

Bosch F. and Müller I. 2005. Improved karst exploration by VLF-EM gradient surveys: comparison with other geophysical methods. *Near Surface Geophysics* **3**, 299–310.

Carreon-Freyre D. and Cerca M. 2006. Delineating the near-surface geometry of the fracture system affecting the valley of Querétaro, Mexico: Correlation of GPR signatures and physical properties of sediments. *Near Surface Geophysics* **4**, 49–55.

Cunningham K. 2002. Application of ground-penetrating radar, digital optical borehole images, and cores for characterization of porosity hydraulic conductivity and paleokarsts in the Biscayne aquifer, southeastern Florida. *Journal of Applied Geophysics* **55**, 61–76.

Danbom S. 2005. Techniques to evaluate shallow karst features. In: *Special Challenges Associated wit the Near Surface* (ed. D. Butler), pp. 13-22. SEG.

Darnault C.J.G. 2008. Karst aquifers: Hydrogeology and exploitation. In: *Overexploitation and Contamination of Shared Groundwater Resources Management, (Bio) Technological, and Political Approaches to Avoid Conflicts* (ed. C.J.G. Darnault), pp. 203–226. NATO Science for Peace and Security Series C: Environmental Security, Springer.

Debeglia N. and Dupont F. 2002. Some critical factors for engineering and environmental microgravity investigations. *Journal of Applied Geophysics* **50**, 435–454.

Doll W., Nyquist J., Beard L. and Gamey T. 2000. Airborne geophysical surveying for hazardous waste site characterization on the Oak Ridge Reservation, Tennessee. *Geophysics* **65**, 1372–1387.

Doolittle J. and Collins M. 1998. A comparison of EM and GPR methods in areas of karst. *Geoderma* **85**, 83–102.

Ford D.C. and Williams P. 2007. *Karst Hydrogeology & Geomorphology*. Wiley & Sons.

Gamey T.J., Thompson M., Mandell W. and Frano G. 2001. Karst pathway delineation using combined spatial and geophysical analysis at Camp Crowder, Missouri. GSA Annual Meeting, 5–8 November 2001, Boston, Massachusetts.

Gamey T.J., Thompson M., Mandell W., Frano G. and Miller S. 2002. Karst pathway delineation using combined spatial and geophysical analysis at Camp Crowder, Missouri. Proceedings of the SAGEEP 2002, Expanded Abstracts.

Garmann K. and Purcell S. 2004. Application for capacitively coupled resistivity surveys in Florida. *The Leading Edge* **23**, 697–698.

Groom R. and Alvarez C. 2002. 3D EM modelling application of the localized non-linear approximator to near surface applications. Proceedings of the SAGEEP 2002, Expanded Abstracts.

Guérin R. and Benderitter Y. 1995. Shallow karst exploration using MT-VLT and DC resistivity methods. *Geophysical Prospecting* **43**, 635–653.

Henson H., Sexton J., Henson M. and Jones P. 1997. Georadar investigation of karst in a limestone quarry near Anna. 67th SEG meeting, Dallas, Texas, USA, Expanded Abstracts, 763–767.

Huang H. 2008. Airborne geophysical data leveling based on line-to-line correlations. *Geophysics* **73**, F83–F89.

Krekeler M.P.S., Probst P., Samsonov M., Tselepis C.M., Bates W., Kearns L.E. and Maynard B. 2007. Investigations of subsurface flow constructed wetlands and associated geomaterial resources in the Akumal and Reforma regions, Quintana Roo, Mexico. *Environmental Geology* **53**, 709–726.

Lesser J.M. 1976. Estudio hidrogeologico e hidrogeoquimico de la peninsula de Yucatan. Unpublisched Technical Report. Proyecto Conacyt-NSF 704, Secretaria de Recursos Hidraulicos, Direccion de Geohidrologia y Zonas Aridas, Mexico.

Loke M.H. and Dahlin T. 2002. A comparison of the Gauss-Newton and quasi-Newton methods in resistivity imaging inversion. *Journal of Applied Geophysics* **49**, 149–162.

Mandell W., Gamey T.J. and Doll W. 2003. Groundwater pathway mapping using airborne geophysics: Two case studies. Proceedings of the the Sixth International Symposium and Exhibition on Environmental Contamination in Central and Eastern Europe and the Commonwealth of Independent States, Prague 2003.

McGath R.J., Syles P., Thomas E. and Neale S. 2002. Integrated high-resolution geophysical investigations as potential tools for water resource investigations in karst terrain. *Environmental Geology* **42**, 552–557.

Mingelli C. 1989. Application of the geoelectrical prospecting method for detection of Karst cavities. 59th SEG meeting, Dallas, Texas, USA, Expanded Abstracts, 424.

Morales J. J. 1992. *Los humedales, un mundo olvidado*. Amigos de Sian Ka'an, Cancun.

Morales J. J. 1993. *El mar y sus recursos*. Amigos de Sian Ka'an, Cancun.

Morales J. J. 1995. *La Gran Selva Maya*. Amigos de Sian Ka'an, Cancun.

Motschka K. 2001. Aerogeophysics in Austria. *Bulletin of the Geological Survey of Japan* **52**, 83–88.

Murray I.R., Alvarez C. and Groom R.W. 1999. Modelling of complex electromagnetic targets using advanced non-linear approximator techniques. 69th SEG meeting, Houston, Texas, USA, Expanded Abstracts.

Nyquist J.E., Peake J.S. and Roth M.J.S. 2007. Comparison of an optimized resistivity array with dipole-dipole soundings in karst terrain. *Geophysics* **72**, F139.

Nyquist J., Petruccione J. and Roth M. 1999. Characterization of shallow karst terrain using multifrequency electromagnetic induction: Two examples from eastern Pennsylvania. 69th SEG meeting, Houston, Texas, USA, Expanded Abstracts, 547–550.

Pankratov O.V., Kuvshinov A.V. and Avdeev D.B. 1997. High performance three-dimensional electromagnetic modelling using modified Neumann series. Anisotropic Earth. *Journal of Geomagnetism and Geoelectricity* **49**, 1541–1547.

Roth M., Mackey J., Mackey C. and Nyquist J. 2002. A case study of the reliability of multielctrode earth resistivity testing for geotechnical investigations in karst terrains. *Engineering Geology* **65**, 225–232.

Sengpiel K. and Siemon B. 1998. Examples of 1-D inversion of multifrequency HEM data from 3-D resistivity distributions. *Exploration Geophysics* **29**, 133–141.

Smith B.D., Gamey J.T. and Hodges G. 2005. Review of airborne electromagnetic geophysical surveys over karst terrains. Proceedings of the US Geological Survey Karst Interest Group, Rapid City, South Dakota, 12–15 September.

Smith B.D., Irvine R., Blome C., Clark A. and Smith D.V. 2003. Preliminary results, helicopter electromagnetic and magnetic survey of the Seco Creek area, Medina and Uvalde counties, Texas. Proceedings of SAGEEP 2003, Expanded Abstracts.

Smith B.D., Smith D.V. and Blome C.D. 2008. Helicopter electromagnetic surveys of carbonate karstic aquifers with emphasis on recent applications by the US Geological Survey. Proceedings of the 5th International Conference on Airborne Electromagnetics (AEM2008), Haikko Manor, Finland.

Steinich B. and Marín L. 1997. Determination of flow characteristics in the aquifer of the Northwestern Peninsula of Yucatan, Mexico. *Journal of Hydrobiology* **191**, 315–331.

Williams P.W. 1993. Environmental Change and Human Impact on Karst Terrains: An Introduction. Catena Supplement 25.Catena Verlag, Cremlingen-Destedt, Germany.

Zhang Z., Routh P.S., Oldenburg D.W., Alumbaugh D.L. and Newman G.W. 2000. Reconstruction of 1-D conductivivty from dual loop EM data. *Geophysics* **65**, 492–501.

Zhou W., Beck B. and Adams A. 2002. Effective electrode array in mapping karst hazards in electrical resistivity tomography. *Environmental Geology* **42**, 922–928.